



## CORRESPONDENCE

### Comments on “The Gulf Stream Convergence Zone in the Time-Mean Winds”

RIWAL PLOUGONVEN, ALEXIS FOUSSARD, AND GUILLAUME LAPEYRE

*Laboratoire de Météorologie Dynamique/IPSL, Ecole Polytechnique, Palaiseau, and CNRS, and Ecole Normale Supérieure, PSL Research University, Paris, and Ecole des Ponts ParisTech, Champs-sur-Marne, France*

(Manuscript received 30 November 2017, in final form 28 February 2018)

#### ABSTRACT

In a recent study, O'Neill et al. analyzed the divergence of surface winds above the northwest Atlantic. In the time mean, a band of convergence is found, overlying the southern flank of the Gulf Stream. To quantify the impact of synoptic storms, the authors proposed to compare the time-mean divergence with the divergence averaged in the absence of rain. In the resulting conditional-average field, divergence was found to be positive nearly everywhere. O'Neill et al. concluded that this absence of convergence precludes the Ekman-balanced mass adjustment to be responsible for the atmospheric response above the Gulf Stream. Using a simplistic toy model as well as a numerical simulation representative of a storm track, we show that the absence of negative divergence values purely results from the correlation between rain and convergence: the conditional average based on the absence of rain necessarily implies a shift toward positive divergence values. In consequence, we argue that conditional statistics (based on the absence of rain or removing extreme values in the divergence field), as produced by O'Neill et al., do not allow conclusions on the mechanisms underlying the atmospheric response to the Gulf Stream. They nevertheless highlight the essential role of synoptic storms in shaping the divergence field in instantaneous fields.

#### 1. Introduction

O'Neill et al. (2017, hereinafter ON17) have recently presented a detailed analysis on the relation between surface divergence and the underlying sea surface temperature (SST) anomalies, drawing from a 10-yr record of satellite measurements and from a 1-yr simulation with a regional model. Their focus was on the relation between the time-mean surface divergence and the fluctuations associated with passing storms. Indeed, the time-mean divergence of surface winds (or of surface stress on the ocean) has been abundantly studied in the past decade, showing a conspicuous relation to SST (Small et al. 2008; Bryan et al. 2010 and references therein). In particular, Minobe et al. (2008) convincingly showed that there is convergence on the warm flank of the Gulf Stream and divergence on the cold flank. Yet this time-mean divergence is of order  $10^{-5} \text{ s}^{-1}$ , that is, one order of magnitude weaker than the maximum instantaneous values

found in the divergence field (of order  $10^{-4} \text{ s}^{-1}$ ). These extreme values of surface divergence are often negative values (i.e., convergence) tied to surface fronts and the associated resulting convection (e.g., Fig. 4 of ON17).

ON17 have used different approaches and filters to isolate the contribution of storms to the time-mean signature in divergence. Their systematic analysis provides a novel and valuable outlook on an important aspect of the effect of SST on atmospheric dynamics. Indeed, different mechanisms have been proposed to explain the relation between SST and the overlying winds. On the one hand, the vertical momentum mixing mechanism relies on the vertical stability of atmospheric boundary layer over SST anomalies (Businger and Shaw 1984; Hayes et al. 1989; Chelton et al. 2004). On the other hand, a pressure adjustment mechanism relies on the hypothesis that the boundary layer is in an Ekman-like balance (Lindzen and Nigam 1987; Feliks et al. 2004; Minobe et al. 2008; Lambaerts et al. 2013). However, the related studies have often focused on the time-mean fields, and the interplay of different mechanisms in instantaneous complex flow fields remains unclear.

*Corresponding author:* Riwal Plougonven, riwal.plougonven@polytechnique.edu

DOI: 10.1175/JAS-D-17-0369.1

© 2018 American Meteorological Society. For information regarding reuse of this content and general copyright information, consult the [AMS Copyright Policy](http://www.ametsoc.org/PUBSReuseLicenses) ([www.ametsoc.org/PUBSReuseLicenses](http://www.ametsoc.org/PUBSReuseLicenses)).

This problem falls in a broader category of problems common in geophysical fluid dynamics, in which a weak time-averaged signal is dwarfed in any instantaneous flow field by temporary fluctuations. As other examples, one may think of the Hadley circulation, mean currents in the ocean that are often dominated by the mesoscale eddy field, or the Brewer–Dobson circulation (Butchart 2014), for which the ascending motion in the tropics can only be indirectly inferred, because the associated vertical velocities are dwarfed by the signatures of equatorial waves in any snapshot of the flow field.

We wish to build on the analysis of ON17 and to point out an aspect of the method used in their paper that needs to be emphasized. Indeed, part of the conclusions put forward by ON17 relies on the computation of conditional averages of different fields. However, part of the interpretation of these statistics is not justified. Specifically, they claim that, because of the absence of convergence in “rain free” conditions (occurring between 80% and 90% of the time; see Fig. 2 of ON17), an “Ekman-balanced mass adjustment” (EBMA) mechanism cannot be at work. The underlying premise is that this mechanism should be “persistent” and therefore be present even when averaging over a subset of times, especially a large subset.

The present comment aims merely to point out that conditional averages and other similar filters that are considered by ON17 introduce a bias, because the variable used for the condition is strongly correlated to the variable that is averaged. In the present case, it is not the sign of the averaged divergence that is meaningful but rather its spatial variations. With that in mind, there is no longer a straightforward transition from ON17’s results to an interpretation in terms of mechanisms. Nonetheless, we acknowledge that the study of ON17 has the merit of unveiling the possible role of synoptic storms in shaping the different mechanisms at work in instantaneous winds.

In section 2, a toy model is proposed to illustrate the difficulty in diagnosing the behavior of the marine atmospheric boundary layer (MABL) and storms in instantaneous or time-mean winds. An idealized simulation of storm tracks carried out with the WRF Model is then investigated in section 3, to further illustrate and confirm the statements of section 2 but also to explore how the time-mean divergence may result from a combination of mechanisms. Implications and directions for further research are discussed in section 4.

## 2. A toy model for illustrating conditional averages

To clarify the interpretation of the observations and model simulations carried out by ON17, we propose to consider a very simplified model.

### a. On the sign of the average divergence

Many of the conclusions of ON17 come from the fact that the conspicuous band of *convergence* on the southern flank of the Gulf Stream vanishes when divergence is averaged for rain-free conditions only (their Fig. 1b) or when other filters retaining rain events are used (their Figs. 5b and 8b). It is the disappearance of the negative values (in green with their color bar) that they emphasize. ON17 deduce “that the existence of the Gulf Stream convergence zone in the time-mean winds owes its existence to extreme storm convergences, since removing a relatively small number of data points associated with storms removes the time-mean convergence” (ON17, p. 2397). This line of reasoning bears a fundamental flaw, as the conclusions of ON17 are mainly based on the *sign* of the rain-free time-mean convergence. In fact, it can be shown that any conditional average (here, rain-free conditions) will systematically introduce a positive or negative (here, positive) bias in the variable that is averaged (here, divergence) if this variable is statistically correlated with the chosen condition. The positive bias arises because rain and surface divergence are not dynamically independent. Hence, the sign of the conditionally averaged divergence is not necessarily meaningful.

### b. Toy model

A toy model is proposed below with the purpose of illustrating how a conditional average can shift the values of divergence toward positive or negative values, suggesting a different interpretation of ON17’s figures. In the present case, our toy model is constructed such that a stationary, weak convergence coexists with random fluctuations that dominate the signal at any time but do not impact the long-term average. This toy model mimics two physical properties of the fields that are considered:

- 1) Rain and surface divergence are not independent variables: convective rain events are associated with mesoscale motions, which include strong convergence roughly beneath the precipitating cell.
- 2) In the boundary layer, over a sufficiently long time and over a wide-enough region, there is no net export or import of air. In other terms, strong convergence must be compensated by divergence in other locations.

The toy model describes the divergence spatial field, assuming that it consists of a permanent feature and random fluctuations that resemble convective events (rain associated with strong convergence values). To simplify, we consider only one-dimensional signals, noted  $d(y, t)$ , where  $y$  is a spatial dimension (e.g., transverse to a front

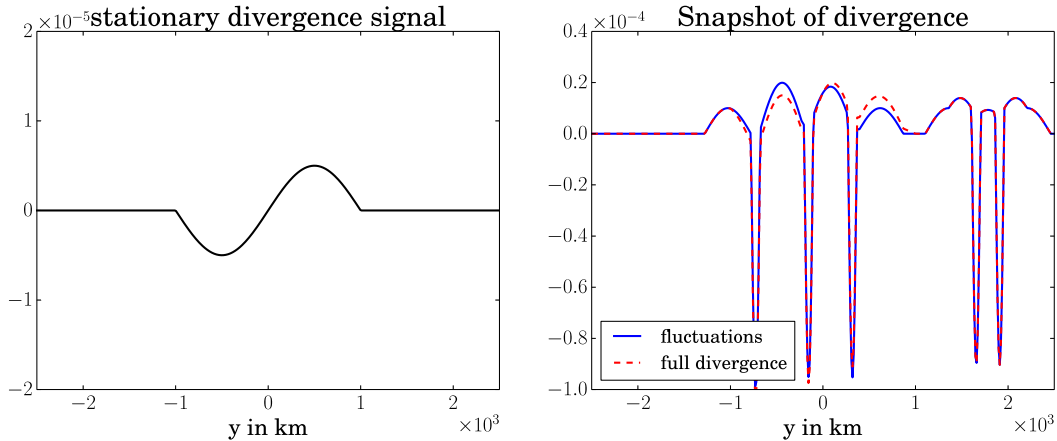


FIG. 1. (left) The stationary divergence  $d_p(y)$  ( $s^{-1}$ ). (right) Snapshot of the fluctuating component  $d_s(y, t)$  (blue line;  $s^{-1}$ ) and of the resulting full divergence signal  $d(y, t)$  (red dashed line;  $s^{-1}$ ). Note the different vertical scale relative to (left).

of sea surface temperature) and  $t$  is time. We assume that the divergence field is the sum of a permanent component  $d_p(y)$  and fluctuations  $d_s(y, t)$  composed of several individual “storms” at each time, centered at random locations  $y_c(t)$  but all with the same spatial shape (see the [appendix](#)):

$$d(y, t) = d_p(y) + d_s(y, t). \quad (1)$$

Note that no assumption on the physical origin of the permanent signal is required in the following development, as we only want to stress our difficulties in interpreting conditional averages.

We also consider that, at any particular time,  $d_p$  and  $d_s$  integrate to zero over the domain of interest and that storms occur at random locations with uniform probability so that they cancel out in the long run. In this case, the long-time-averaged divergence yields  $d_p(y)$

$$\bar{d}(y) = \lim_{T \rightarrow \infty} \frac{1}{T} \int_0^T d(y, t') dt' \rightarrow d_p(y). \quad (2)$$

Using simple sinusoidal functions, an implementation has been carried out; details are given in the [appendix](#). For simplicity, at each time step, five “storm” centers are defined at random (uniformly distributed) locations in the domain (of length  $2D = 5000$  km). Each storm consists in a region of convergence of maximal magnitude  $a = 1.0 \times 10^{-4} s^{-1}$  and of width  $2l = 100$  km, compensated by weaker divergence of maximal magnitude  $1.0 \times 10^{-5} s^{-1}$  and over a width  $L = 500$  km on both sides. The stationary signal has a smaller magnitude, of  $0.5 \times 10^{-5} s^{-1}$ . [Figure 1](#) illustrates the stationary signal ([Fig. 1a](#)) and a typical instantaneous divergence field ([Fig. 1b](#)). It confirms that the stationary signal is dwarfed at any time by the intermittent signal from the fluctuations with much larger amplitude.

In [ON17](#), the conditional average is taken over rain, which is related in some proportion to divergence. To represent this, we produce an intermediate field  $r(y, t) = -d_s(y, t) + \eta$ , where  $\eta$  is a random Gaussian noise [to make the field  $r(y, t)$  more similar to rain, one could set all its negative values to zero]. The conditional average is then taken using the condition  $r > 0$  (rain only) or  $r \leq 0$  (rain free). [Figure 2a](#) illustrates the resulting averages obtained for different numbers of time steps used. In the overall average, the stationary signal  $d_p(y)$  is recovered (note that a signal different from  $d_p$  is observed near the boundaries of the domain because of a finite-domain effect). In the rain-free average, the same signal is recovered but shifted to positive values. The shift is sufficient that all values [even in the region of convergence for  $d_p(y)$ ] become positive. In other words, this shift, or positive bias, is larger than the amplitude of  $d_p(y)$ . The rain-only signal is shifted to strongly negative values; again, the spatial structure is unaltered, but it is hidden in the noise unless a long time average is taken.

The conclusion from this figure is that the conditional average (in the setting of this toy model) shifts the rain-free average toward positive values but without altering its spatial structure. Moreover, as the rain-free average excludes the intense values (tied to storms), it is less noisy than the overall average. The rain-only average including mainly extreme events is by construction very noisy.

### c. The positive bias

We now take advantage of the simplicity of this toy model to quantify, in this case, the amplitude of the positive bias. This can be calculated simply in the case when there is no noise; that is, we average conditionally on the sign of  $d_s(y, t)$ , and we consider only one storm

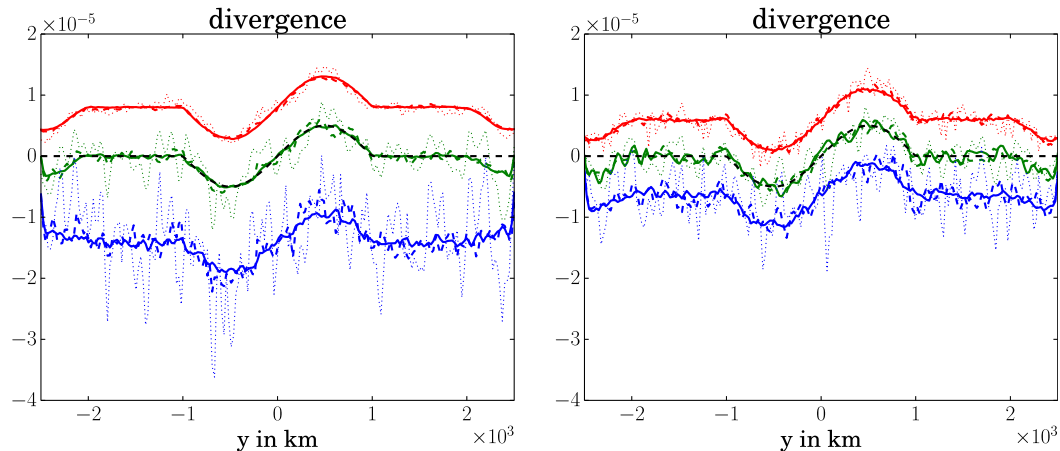


FIG. 2. (left) Time-mean divergence of the toy model, averaged over 10 000 (thick lines), 1000 (dashed lines), and 100 time steps (dotted lines). The green lines correspond to total averages, whereas the blue lines correspond to rain-only and the red lines correspond to rain-free conditional averages. (right) As in (left), but with a noise level of  $\sigma = 5 \times 10^{-5} \text{ s}^{-1}$  instead of  $\sigma = 1 \times 10^{-5} \text{ s}^{-1}$ . In both panels, the black dashed curve is  $d_p$ . Parameters used for the toy model are given in the [appendix](#).

per time step. The storm locations being uniformly distributed and the spatial shape of  $d_s(y, t)$  being fixed, the “rain frequency”  $\chi = p(\text{rain} > 0)$  is uniform across the domain and is given by the ratio of the width of the convergent region ( $d_s < 0$ ) over the width of the domain, 2D, such that  $\chi = l/D$ . The form given to the convergence is such that its average value computed over the convergence zone is  $-2a/\pi$ . Hence, the rain-only average is

$$\bar{d}^{\text{RO}}(y) = d_p(y) - \frac{2a}{\pi}. \quad (3)$$

As all times are partitioned into rain free and rain only, one necessarily verifies  $\bar{d} = \bar{d}^{\text{RF}}(1 - \chi) + \bar{d}^{\text{RO}}\chi$ , and the rain-free average can be calculated as

$$\bar{d}^{\text{RF}}(y) = d_p(y) + \frac{2a}{\pi} \frac{l}{D - l}. \quad (4)$$

The above gives an estimate of the systematic biases introduced by the conditional averaging in the absence of noise, that is, when  $r(y, t) = -d_s(y, t)$ . When a random noise is present, rain and divergence have a less simple relation but are correlated. As the noise increases, the biases decrease in absolute value from their values obtained above, and the asymmetry between rain-free and rain-only means decreases, as illustrated from [Fig. 2b](#). Nonetheless, because the signature in convergence of the rain events is much larger than that of the stationary signal,  $a \gg \max[d_p(y)]$ , and despite the fact that they occupy a small portion of space [ $l/(D - l) \sim l/D \ll 1$ ], it is likely that the positive bias is sufficient to shift the whole signal of  $\bar{d}^{\text{RF}}$  to positive values.

The point that the above toy model illustrates is that the absence of convergence in the rain-free conditional average [ $\bar{d}^{\text{RF}}(y) > 0$ ] does not rule out the presence of a stationary signal in the divergence field. It merely reflects that divergence and rain are strongly correlated, as illustrated by [ON17](#) (see their [Fig. 4c](#)). We return to this issue below and in [section 4](#).

### 3. Idealized atmospheric simulation

To bridge the gap between the maps displayed by [ON17](#) and the one-dimensional illustrations from our toy model, we here take advantage of a simulation carried out for investigating the atmospheric response to mesoscale SST anomalies (A. Foussard et al. 2018, unpublished manuscript). It consists of an idealized setup of a midlatitude storm track using the WRF Model ([Skamarock et al. 2008](#)) in a zonally periodic channel and using a gray radiation scheme ([Frierson et al. 2006](#)). The domain is 9216 km in both horizontal directions and extends up to about 20 km (50 hPa) in height. The horizontal resolution ( $dx = 18 \text{ km}$ ) allows a good description of atmospheric storms, leading to a reasonable storm track. Boundary layer processes are represented by the Yonsei University (YSU) scheme, convection by the Kain and Fritsch scheme, and microphysics by the Kessler scheme. The fixed zonally symmetric SST distribution in the simulation presented here consists of a large-scale meridional gradient with maximal amplitude of  $4 \text{ K} (100 \text{ km})^{-1}$ . The simulation has been carried out for 4 years, and the first 90 days were discarded. Data were recorded every 12 h.

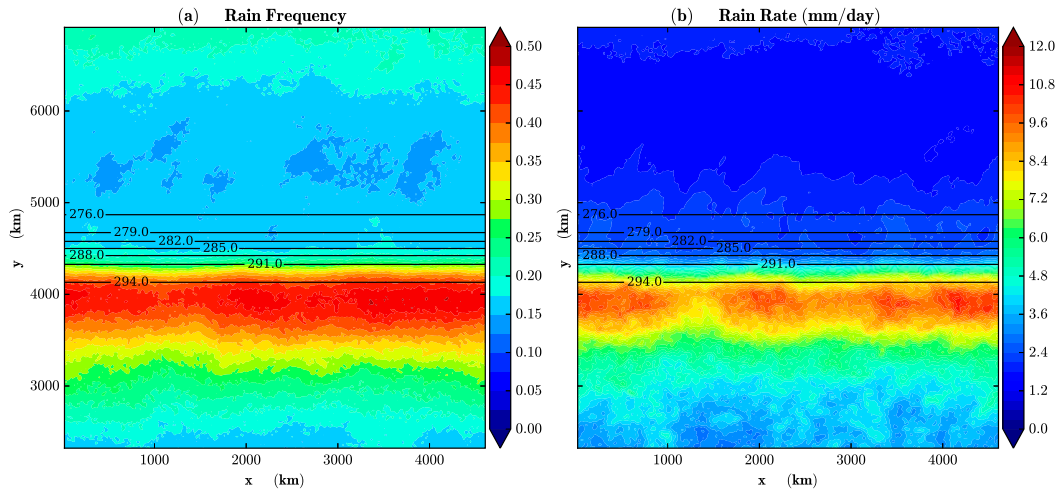


FIG. 3. Mean rain frequency and mean rain rate ( $\text{mm day}^{-1}$ ) over the 4 years. Contours show the SST field (K). All calculations have been made considering rain rates over 12 h of larger than  $3 \text{ mm day}^{-1}$ .

*a. Conditional averages of surface divergence*

Figure 3 shows the rain frequency and the mean rain rate over the whole domain, clearly indicating a preferred location for rain that is south and away from the SST front. This may be compared with Fig. 2 of ON17, the comparison suggesting that our simulation has a realistic mean rain rate but overestimates the maximum rain frequency and the meridional contrast in rain frequency over the SST front. This does not matter for the present purpose, which is again to illustrate the systematic bias introduced by the conditional averages and by other similar filters.

Figure 4 shows the time average and conditional averages of the surface divergence, as in Fig. 1 of ON17. The mean surface divergence (Fig. 4a) shows a pattern with convergence south of the SST front and divergence over the SST front and to the north of it, analogous to

that displayed over the Gulf Stream by ON17. Mean values (extremes of about  $\pm 0.4 \times 10^{-5} \text{ s}^{-1}$ ) are quite comparable to the values found from observations. For the conditional averages, as expected, the rain-free divergence is shifted to positive values in all locations (Fig. 4b), whereas the rain-only divergence is shifted to only negative values (Fig. 4c).

Now, one advantage of this idealized setting is the zonal symmetry of the underlying SST, allowing us to average easily in the alongfront direction. This averaging leads to the same presentation as for the toy model of section 2. Figure 5 shows the zonally averaged time-mean surface divergence along with the rain-free and rain-only conditional averages. In addition, the underlying Laplacian of SST is also displayed as an indication of area where surface convergence is expected in the EBMA theory. Again, it is clearly seen that the conditional average displaces the rain-free average to

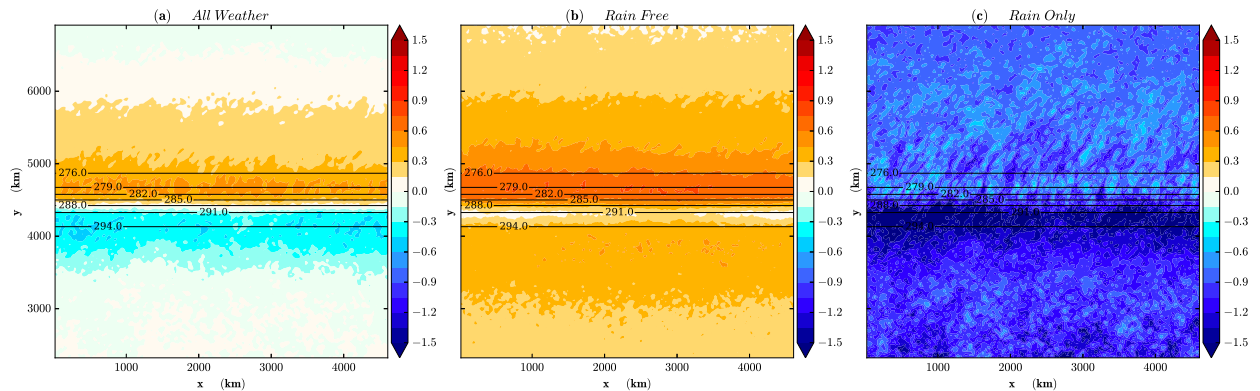


FIG. 4. Surface divergence (colors;  $10^{-5} \text{ s}^{-1}$ ) considering (a) an unconditional mean, (b) a rain-free conditional mean, and (c) a rain-only conditional mean. Contours show the SST field (K).

positive values and the rain-only average to negative values. Both conditional averages retain some of the spatial structure present in the all-weather average, but there are also notable differences. For example, in the rain-free average, the central couplet occurs on shorter spatial scales than in the all-weather average. The meaning and interpretation of these differences are not the purpose of the present comment and would anyhow be tied to specificities of these idealized simulations. The important message is that the conditional average of divergence, conditioned on a variable with which divergence is correlated, leads to a bias that makes the convergent values disappear from the rain-free average. The disappearance of these convergent values does not allow the interpretation made by ON17, that is, that a stationary (or permanent or persistent) feature is absent from the divergence field.

The same simulation can be used to illustrate another analysis made by ON17, bearing on the statistics of divergence. The skewness of the divergence distribution was emphasized as a crucial parameter (e.g., ON17, section 6). As a complement to the conditional averages, ON17 examined the average of divergence when extreme values (away from the mean by more than twice the standard deviation,  $2\sigma$ ) are excluded or when only extreme values are retained (ON17, their Fig. 5). This was not explored in the toy model because the distribution of divergent values in there was not tied to a physical description of the processes. In the numerical simulation with a mesoscale model, it becomes meaningful to explore this distribution. Figure 6 shows maps of the mean divergence overall and filtered divergence excluding extreme values or retaining only those. The format for the first four panels is the same as that of Fig. 5 of ON17. As shown by Fig. 6d, the  $2\sigma$  filter removes a comparable amount of data (4%–5%) in the area of maximum convergence. Again, the maps are very similar to the rain-free and rain-only means. In particular, the mean divergence excluding extreme values (Fig. 6b) is positive essentially everywhere, as is the rain-free mean (Fig. 4b). Yet, as we saw previously, it is not the sign of the mean divergence that is meaningful but the spatial variations: in both cases, the rain-free divergence did retain conspicuously part of the spatial variations present in the overall time mean. In Figs. 6e and 6f, the averaged divergences excluding or retaining extreme values are presented but removing their domain average. It then becomes apparent that the former includes spatial variations very similar to those of the mean divergence but slightly weaker. In contrast, the mean retaining only extreme events consists only of a strong band of convergence, wider than that of the overall mean divergence, and without the positive

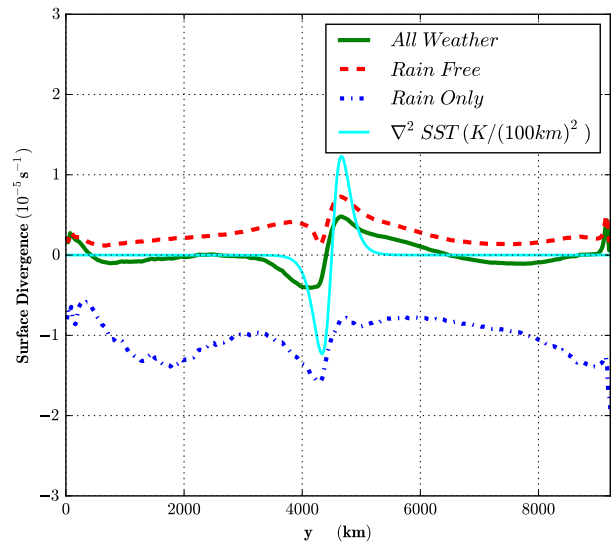


FIG. 5. Zonally averaged unconditional and conditional means of surface divergence ( $10^{-5} \text{ s}^{-1}$ ). Same quantities as in Fig. 4, considering the zonal mean of the signals. The light blue line is the Laplacian of SST ( $10^{-10} \text{ K m}^{-2}$ ).

counterpart to the north. These different spatial structures and relative amplitudes can be better appreciated from the zonally averaged description of these means in Fig. 7 rather than in maps where the choice of colors guides the eye and interpretation. It would be very informative in ON17 if their Figs. 1 and 5 were complemented with similar figures: for example, instead of presenting only the rain-free mean divergence, if a panel was included to show the rain-free mean divergence minus the spatial average over the area shown. Alternatively, the rain-free divergence could be shown with contours overlaid to the overall mean divergence, so one could see if the spatial variations and features coincide (but the comparison of the amplitudes would remain difficult).

### b. Statistics of divergence values

Finally, we use the simulation to explore the overall distribution of the values taken by the divergence, similar to ON17 in their Fig. 6. The distribution of divergent values in our simulation is shown in Fig. 8a, showing good qualitative agreement with the distribution displayed from observations by ON17. In particular, we also find that large positive values of divergence are more frequent in rain-only conditions than in rain-free conditions, implying that there is not systematically convergence below rain. But we emphasize that the large positive values are one order of magnitude less likely than negative values. Now it was stressed several times above that divergence and rain are not dynamically independent and that they are statistically

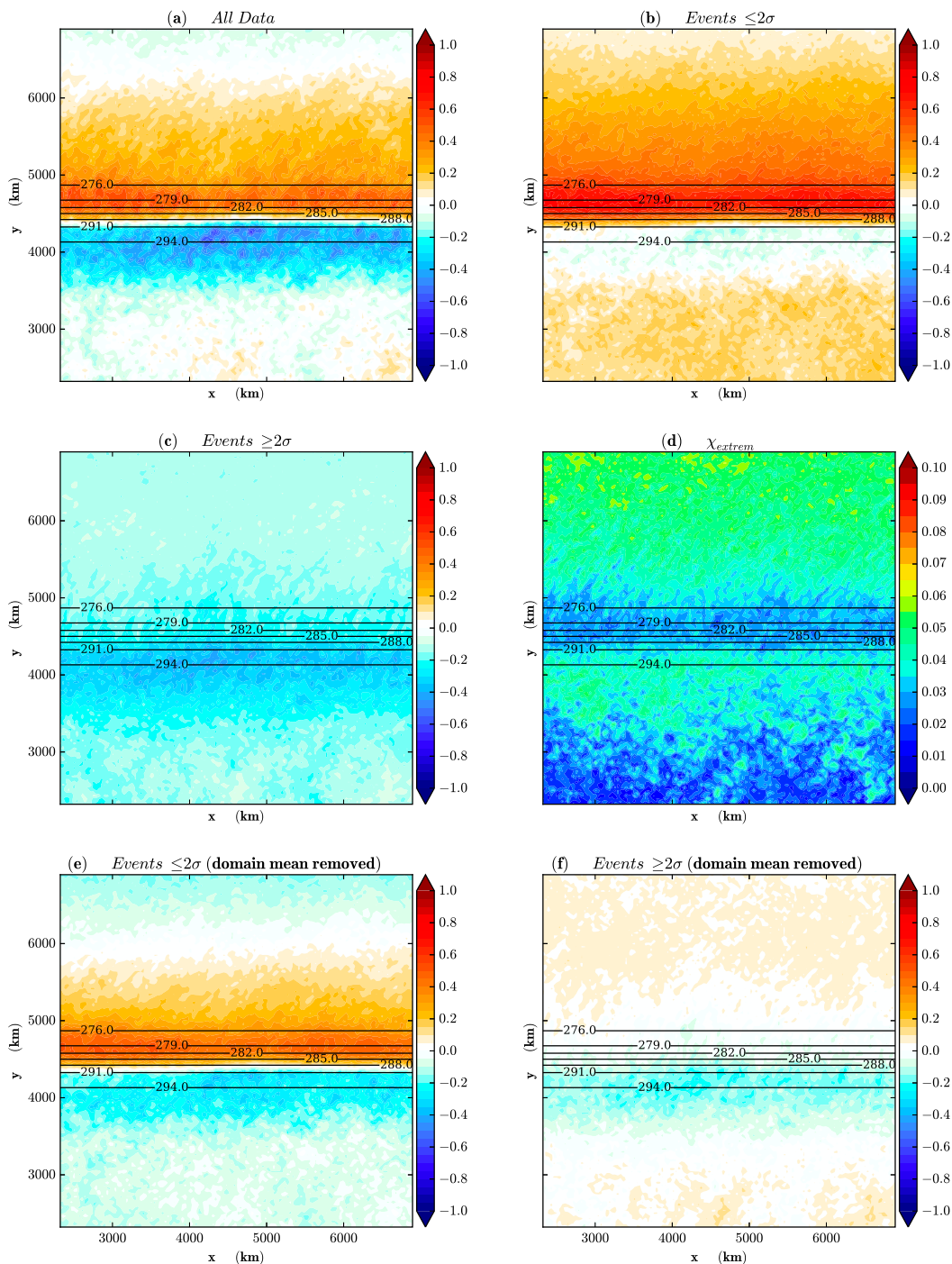


FIG. 6. Mean surface divergence (shading;  $10^{-5} \text{ s}^{-1}$ ) (a) for the whole time series, (b) with values smaller than  $2\sigma$ , and (c) with only values larger than  $2\sigma$ . (d) Fraction of points with deviation from the mean bigger than the  $2\sigma$  threshold. (e),(f) As in (b) and (c), respectively, after subtracting out the domain-averaged signal. Contours show the SST field (K).

correlated. The simulation makes it possible to document the joint probability distribution function of divergence and rain, shown in Fig. 8b. The mean divergence, for a given value of rain, is negative and

increasingly negative as the rain value increases, as shown by the blue line. This gives another a posteriori justification of the setup of the toy model, where the intermediate rain field has been built by adding random

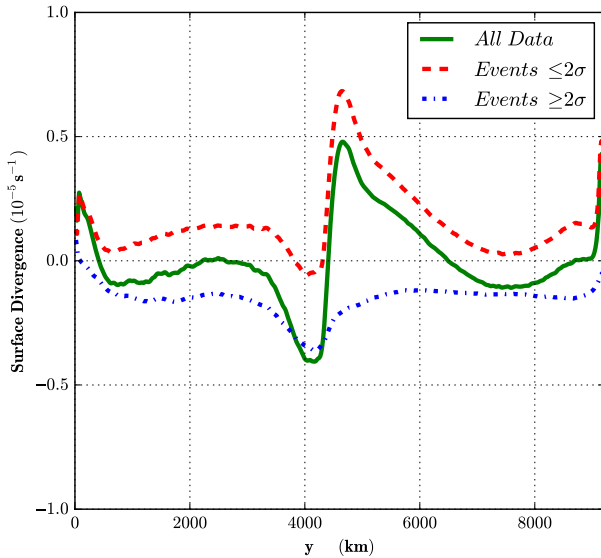


FIG. 7. Unfiltered and filtered surface divergence ( $10^{-5} \text{ s}^{-1}$ ). Same quantities as in Figs. 6a–c, considering the zonal mean of the signals.

noise to the divergence. This also makes it possible to revisit how the sign of the rain-only mean divergence is determined. If we write  $p(e) de$ , the probability that the divergence takes a value between  $e$  and  $e + de$ , the overall mean divergence can be written as

$$\bar{d} = \int_{-\infty}^{+\infty} ep(e) de. \quad (5)$$

The rain-only mean divergence (calculated using only values of rain above a threshold  $\varepsilon$ ) is then written as

$$\bar{d}^{\text{RO}} = \frac{\int_{-\infty}^{+\infty} ep(e|\text{rain} > \varepsilon) de}{\int_{-\infty}^{+\infty} p(e|\text{rain} > \varepsilon) de}. \quad (6)$$

In the integrand of the numerator in Eq. (6), one may decompose the conditional probability on rain being larger than the threshold  $\varepsilon$  and write it as the sum of the conditional probabilities knowing that rain is within interval  $[r, r + dr]$ :

$$p(e|\text{rain} > \varepsilon) = \int_{\varepsilon}^{+\infty} p(e|r \leq \text{rain} < r + dr)q(r) dr, \quad (7)$$

with  $q(r)$  the probability density function for the rain rate. This yields

$$\begin{aligned} \bar{d}^{\text{RO}} &= \frac{\int_{-\infty}^{+\infty} e \int_{\varepsilon}^{+\infty} p(e|r \leq \text{rain} < r + dr)q(r) dr de}{\int_{-\infty}^{+\infty} p(e|\text{rain} > \varepsilon) de} \\ &= \frac{\int_{\varepsilon}^{+\infty} q(r) \int_{-\infty}^{+\infty} ep(e|r \leq \text{rain} < r + dr) de dr}{P(\text{rain} > \varepsilon)} \\ &= \frac{\int_{\varepsilon}^{+\infty} q(r)f(r) dr}{P(\text{rain} > \varepsilon)}, \end{aligned} \quad (8)$$

with  $f(r) = \int_{-\infty}^{+\infty} ep(e|r \leq \text{rain} < r + dr) de$ . Up to a normalizing factor,  $f(r)$  is the average divergence knowing the rain rate. This is calculated in our simulation and

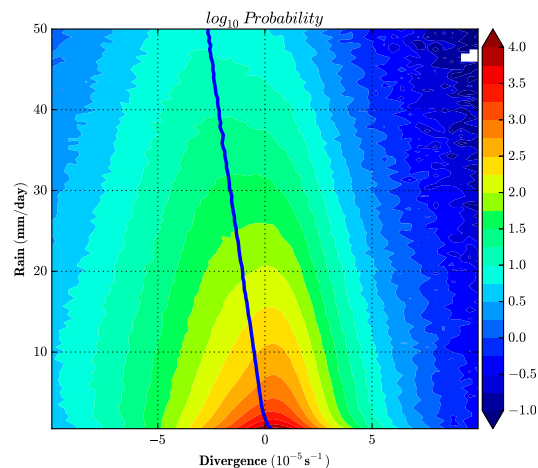
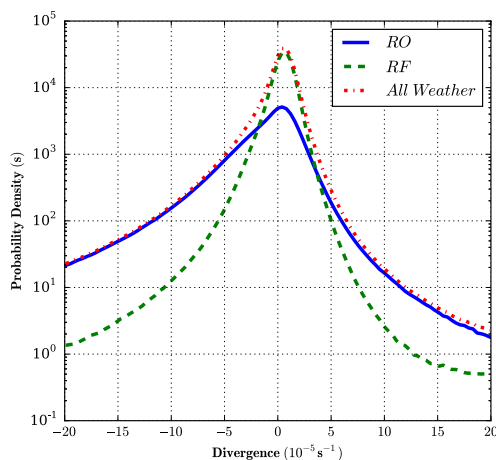


FIG. 8. (a) PDF of the surface divergence (red curve), calculated from all time outputs and for points within a band of latitudes ( $3600 \leq y \leq 5600$  km). Blue and green dashed lines show respective contributions of the rainy and rain-free points to the unconditional PDF. (b) Joint PDF of the rain rate (vertical axis;  $\text{mm day}^{-1}$ ) and the surface divergence (horizontal axis;  $10^{-5} \text{ s}^{-1}$ ). Color scale is logarithmic. The blue line indicates the conditional mean of the surface divergence for a given rain rate.

shown in Fig. 8b as the thick blue line. Consistent with the physical expectation that surface convergence and precipitation are highly correlated, the average divergence knowing the rain rate is always negative for values of rain larger than about  $1 \text{ mm day}^{-1}$  and increasingly negative with increasing precipitation. This clearly demonstrates that the correlation of convergence and precipitation leads to  $\bar{d}^{\text{RO}}$  being negative. As a consequence,  $\bar{d}^{\text{RF}}$  will systematically have a positive shift relative to  $\bar{d}$ . Note that, because strong convergence corresponds to rain-only regions (see Fig. 8a), an analysis based on the  $2\sigma$  filter would lead to the same conclusion. The reason is that the condition still is strongly correlated to the divergence itself.

#### 4. Discussion and perspectives

ON17 conclude from their analysis “that the existence of the GSCZ in the time-mean winds owes its existence to extreme storm convergences, since removing a relatively small number of data points associated with storms removes the time-mean convergence” (ON17, p. 2397). In the conclusion again they state that “strong convergences associated with storms explains the existence of the GSCZ in the time-mean surface winds” (ON17, p. 2409). They explain that the skewness of the surface divergence distribution, due to the strong convergence signatures of midlatitude cyclones, “is sufficient to change the sign of the time mean and the interpretation of the SST influence on divergence. Removing fewer than 4% of the strongest divergence events, or removing fewer than 20% of values in raining conditions, effectively eliminates the GSCZ from the time-mean surface winds” (ON17, p. 2409). The underlying premise is that if the convergence band vanishes when only a small portion of values is removed, this feature cannot be “a persistent feature anchored to the Gulf Stream” (ON17, p. 2404).

We disagree with this premise, but this does not invalidate the entire analysis of ON17 and their conclusions. Our disagreement stems from the too-strong emphasis on the sign of the rain-free divergence. Our study has put in evidence the bias in this sign because of a dynamical link between surface divergence and precipitation that statistically correlates the two fields. As a consequence, the conditional average shifts the rain-free divergence toward positive values and the rain-only divergence toward strongly negative values. The correlation between precipitation and surface divergence is especially true for the most intense values, as can be seen in their Figs. 4b and 4c. The joint probability distribution function (PDF) of convergence and precipitation, as shown in Fig. 8b for our simulation, illustrates clearly this correlation. It would be very

interesting to estimate this joint PDF from observations. Yet, as far as the color bars in their Figs. 1, 5, and 13 allow us to judge, much of the spatial variations between the rain-free and all-weather divergence coincide. Rather than showing the absolute values of the rain-free and rain-only divergence, showing anomalies (relative either to the mean over the domain or to the field smoothed on large scales) would be less misleading. In the case of the toy model, the same spatial structure came out in the three averages, but the rain-only average is noisier. In the idealized simulation, the spatial structures of the rain-free average have strong resemblance to those of the overall average, whereas those of the rain-only average display some differences.

In the comparisons of their different figures, ON17 emphasize absolute values and discard the similarity that is often found between the spatial variations. For example, the claim of ON17 that the rain-free divergence in their Fig. 13b “bears no resemblance” (ON17, p. 2401) to the SST Laplacian (their Fig. 13h) is at the very least misleading. The spatial variations of both fields, as far as eye can tell, seem very correlated. The colors differ because the rain-free divergence is shifted everywhere to positive values because of the conditional average. Similarly, in the interpretation of their Fig. 11, the strong similarity at spatial scales shorter than 1000 km (their Figs. 11a and 11b) is perhaps more significant than the difference (again a positive shift) in the spatially low-pass-filtered fields (their Figs. 11c and 11d). It is worth emphasizing that on spatial scales shorter than 1000 km (their Figs. 11a and 11b), there is a strong similarity between the time-mean divergence (colors) and the SST Laplacian (contours).

Now, to make progress, we suggest making the line of reasoning of ON17 more explicit and to formulate two different hypotheses:

- 1) Hypothesis 1 (H1): The divergence at any time results from two signals: a stationary signal (related to EBMA) and random fluctuations from storms whose positions vary in time. The signal due to these fluctuations should diminish when averaging over longer times.
- 2) Hypothesis 2 (H2): The divergence at any time only results from storms. The spatial variations of these storms are such that, in the time average, they produce the signature that is observed.

Set in the above terms, ON17 claims that the absence of convergence (negative values) in the rain-free average divergence rules out H1. The toy model of section 2 merely served to illustrate that this conclusion is not justified: it is *possible* to have a rain-free divergence everywhere positive and yet to have a stationary signal

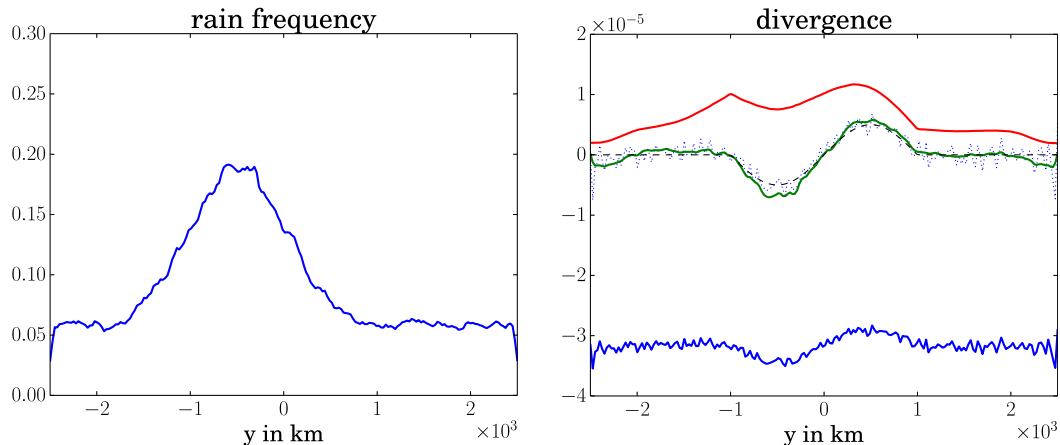


FIG. 9. (left) Rain frequency for the modified toy model. (right) Time-mean divergence of the modified toy model, averaged over 10 000 time steps. The green line corresponds to total averages, whereas the blue line corresponds to  $\bar{d}^{\text{RO}}/2$ , the red line to  $\bar{d}^{\text{RF}}$ , and the dashed black line to  $d_p$ . The blue dotted curve is  $\bar{d}^{\text{RO}}$  minus its spatial average value. It overlaps almost exactly with  $d_p$ . Parameters used for the toy model are given in the appendix.

that is responsible for all of the time-averaged signal. In other words, the absence of *convergence* in the rain-free divergence (or after filtering out extreme values) does not rule out H1 (i.e., the existence of a permanent signal in the divergence).

Now, in our toy model, the shift is uniform in space as the storms were uniformly distributed in space. In contrast to this, in our idealized simulation (see section 3) and in the observations (see Fig. 1c of ON17), the shift is not uniform. Introducing spatial variations in the probability of occurrence of the storms in our toy model (see the appendix for a description of the modifications of the toy model), one observes that storms still leave a residual signal that is related to the stationary divergence term (Fig. 9). Of course, this is on top of another signal due to the localization in space of storms in relation with H2.

Spelling out explicitly the two hypotheses provides two extreme pictures, and reality is likely, as often, in between. The links between the conditional averages analyzed by ON17 and the underlying mechanisms of the atmospheric response to the SST anomalies are not so simple, as illustrated by the present comment. Now, the detailed and extensive analysis carried out by ON17 does emphasize several important points: the instantaneous fluctuations in the divergence field overwhelms the time mean, and understanding this response requires considering how the SST influences storms, in particular in setting their preferred location. We believe that detailed investigations of the instantaneous signature of different mechanisms through which the SST influences the marine atmospheric boundary layer, as sketched in section 5 of ON17, are necessary to properly

evaluate the relevance of these different mechanisms. These issues are complex, as they depend on the variables and approach considered to quantify one or the other mechanism, as will be discussed based on the simulation used in section 3 (A. Foussard et al. 2018, unpublished manuscript).

*Acknowledgments.* This work was granted access to the HPC resources of IDRIS under the allocation for 2015 and 2016 A0010106852 made by Grand Equipement National de Calcul Intensif (GENCI). This research was funded by Agence Nationale de la Recherche Grant SIMI 5-6 014 01.

## APPENDIX

### Implementation of the Toy Model

The toy model we constructed only depends on the divergence fields  $d_p$  and  $d_s$ . We here describe the choices used to implement it. The permanent divergence signal was chosen as

$$d_p(y) = \begin{cases} A \sin\left(\frac{\pi y}{2L}\right), & \text{for } -2L < y < 2L \\ 0, & \text{for } |y| > 2L \end{cases}. \quad (\text{A1})$$

The divergence field is constructed as a sum of  $d_p$  and of five “storms,” each centered at a random (uniformly distributed) location within the domain  $[-D, D]$ . Each event, relative to its central location, has the following spatial structure:

$$g(y) = \begin{cases} \frac{al}{L} \sin \left[ \frac{(y + L + l)\pi}{L} \right], & \text{for } -(L + l) < y < -l \\ -a \cos \left( \frac{y\pi}{2l} \right), & \text{for } -l < y < l \\ \frac{al}{L} \sin \left[ \frac{(y - l)\pi}{L} \right], & \text{for } l < y < L + l \\ 0 & \text{for } |y| > L + l \end{cases}, \quad (\text{A2})$$

where  $-a$  describes the peak intensity of the convergence ( $a > 0$ ),  $l$  describes the width of the convergent region, and  $L$  describes the width of the surrounding regions where compensating divergence occurs. This definition is consistent with our idea that the net divergence would be zero [i.e.,  $\int g(y) dy = 0$ ]. Then  $d_s$  takes the form of

$$d_s(y, t) = \sum_{i=1}^5 g[y - y_c^i(t)], \quad (\text{A3})$$

where  $y_c^i(t)$  is the location of one of the storm centers at time  $t$ .

To obtain the “rain” field  $r(y, t) = -d_s + \eta$ , a random noise  $\eta$  is added. This noise has normal distribution with zero mean and a standard deviation of  $\sigma_{\text{noise}}$ .

The values chosen for the parameters in order to generate the figures were  $A = 0.5 \times 10^{-5} \text{ s}^{-1}$ ,  $a = 1 \times 10^{-4} \text{ s}^{-1}$ ,  $l = 50 \text{ km}$ ,  $L = 500 \text{ km}$ , and  $D = 2500 \text{ km}$ . The number of points in the  $y$  direction is  $n_y = 200$ . Different values for the parameters have been explored. As the noise is increased, the positive bias of the rain-free mean divergence decreases. Nonetheless, as long as the noise is not much larger than  $a$ , the positive bias is robust and significant (i.e., sufficient for the rain-free mean to be positive nearly everywhere).

The model was also modified to show that the same results can be obtained when storms are located on the convergence zone. To this end, we introduce a parameter  $0 < C < 1$ . For each event, we take two random numbers,  $r$  uniformly distributed in  $[0, 1]$  and  $s$  with a Gaussian distribution (centered at 0 and with a variance of 1). The storm position  $y_c$  is then defined as

$$y_p = \begin{cases} (s - 1)L, & \text{if } r < C \\ \left( 2 \frac{r - C}{1 - C} - 1 \right) D, & \text{if } r \geq C \end{cases}. \quad (\text{A4})$$

Figure 9 was produced with this scheme, still using five storms per time step but without noise ( $\sigma_{\text{noise}} = 0$ ) and with 10000 time steps. Parameter  $C$  was set to  $C = 0.4$ . The other parameters were the same as before.

REFERENCES

Bryan, F. O., R. Tomas, J. Dennis, D. Chelton, N. Loeb, and J. McClean, 2010: Frontal scale air–sea interaction in high-resolution coupled climate models. *J. Climate*, **23**, 6277–6291, <https://doi.org/10.1175/2010JCLI3665.1>.

Businger, J. A., and W. J. Shaw, 1984: The response of the marine boundary layer to mesoscale variations in sea-surface temperature. *Dyn. Atmos. Oceans*, **8**, 267–281, [https://doi.org/10.1016/0377-0265\(84\)90012-5](https://doi.org/10.1016/0377-0265(84)90012-5).

Butchart, N., 2014: The Brewer–Dobson circulation. *Rev. Geophys.*, **52**, 157–184, <https://doi.org/10.1002/2013RG000448>.

Chelton, D. B., M. G. Schlax, M. H. Freilich, and R. F. Milliff, 2004: Satellite measurements reveal persistent small-scale features in ocean winds. *Science*, **303**, 978–983, <https://doi.org/10.1126/science.1091901>.

Feliks, Y., M. Ghil, and E. Simonnet, 2004: Low-frequency variability in the midlatitude atmosphere induced by an oceanic thermal front. *J. Atmos. Sci.*, **61**, 961–981, [https://doi.org/10.1175/1520-0469\(2004\)061<0961:LVITMA>2.0.CO;2](https://doi.org/10.1175/1520-0469(2004)061<0961:LVITMA>2.0.CO;2).

Frierson, D. M., I. M. Held, and P. Zurita-Gotor, 2006: A gray-radiation aquaplanet moist GCM. Part I: Static stability and eddy scale. *J. Atmos. Sci.*, **63**, 2548–2566, <https://doi.org/10.1175/JAS3753.1>.

Hayes, S. P., M. J. McPhaden, and J. M. Wallace, 1989: The influence of sea surface temperature on surface wind in the eastern equatorial Pacific: Weekly to monthly variability. *J. Climate*, **2**, 1500–1506, [https://doi.org/10.1175/1520-0442\(1989\)002<1500:TIOSST>2.0.CO;2](https://doi.org/10.1175/1520-0442(1989)002<1500:TIOSST>2.0.CO;2).

Lambaerts, J., G. Lapeyre, R. Plougonven, and P. Klein, 2013: Atmospheric response to sea surface temperature mesoscale structures. *J. Geophys. Res. Atmos.*, **118**, 9611–9621, <https://doi.org/10.1002/jgrd.50769>.

Lindzen, R., and S. Nigam, 1987: On the role of sea surface temperature gradients in forcing low-level winds and convergence in the tropics. *J. Atmos. Sci.*, **44**, 2418–2436, [https://doi.org/10.1175/1520-0469\(1987\)044<2418:OTROSS>2.0.CO;2](https://doi.org/10.1175/1520-0469(1987)044<2418:OTROSS>2.0.CO;2).

Minobe, S., A. Kuwano-Yoshida, N. Komori, S.-P. Xie, and R. J. Small, 2008: Influence of the Gulf Stream on the troposphere. *Nature*, **452**, 206–209, <https://doi.org/10.1038/nature06690>.

O’Neill, L. W., T. Haack, D. B. Chelton, and E. Skyllingstad, 2017: The Gulf Stream convergence zone in the time-mean winds. *J. Atmos. Sci.*, **74**, 2383–2412, <https://doi.org/10.1175/JAS-D-16-0213.1>.

Skamarock, W. C., and Coauthors, 2008: A description of the Advanced Research WRF version 3. NCAR Tech. Note NCAR/TN-475+STR, 113 pp., <https://doi.org/10.5065/D68S4MVH>.

Small, R., and Coauthors, 2008: Air–sea interaction over ocean fronts and eddies. *Dyn. Atmos. Oceans*, **45**, 274–319, <https://doi.org/10.1016/j.dynatmoce.2008.01.001>.